Journal of
Instrumentation

Evaluation of the reliability of Rayleigh scattering as calibration method for the Thomson scattering diagnostic at W7-X

Published by IOP Publishing for Sissa Medialab

Received: *August 30, 2025*
Accepted: *December 25, 2025*
Published: *February 12, 2026*

21st International Symposium on Laser-Aided Plasma Diagnostics
Saillon, Switzerland
1–5 September 2025

Evaluation of the reliability of Rayleigh scattering as calibration method for the Thomson scattering diagnostic at W7-X

J. Wagner[a,*] **G. Fuchert**[a] **K.J. Brunner**[a] **E. Pasch**[a] **J. Knauer**[a] **S.A. Bozhenkov**[a] **M. Hirsch**[a] **R.C. Wolf**[a,b] **and W7-X Team**[1]

[a] *Max Planck Institute for Plasma Physics, Greifswald, Germany*
[b] *Technical University of Berlin, Berlin, Germany*

E-mail: jannik.wagner@ipp.mpg.de

Abstract: Rayleigh scattering is used in an in-situ approach to determine the relative and absolute calibration factors of the Thomson scattering diagnostic at Wendelstein 7-X (W7-X). Using light pulses from an optical parametric oscillator (OPO), it is shown for the first time that the method is allowing for the calibration of all spatial channels (scattering volumes) at once. That has been realized by reducing the high amount of stray light observed in prior attempts. The improved setup is presented and compared to the literature ones. The Rayleigh scattering evaluation is containing the vacuum stray light measurement, which is yielding a rough estimate of the relative calibration without the need of any gas and used for background subtraction and a Rayleigh measurement on argon inside the vessel. The pressure dependency of the Rayleigh contribution in argon is evaluated for two wavelengths in each spectral channel. At the pressure of 377 mbar, the full spectral measurement used for the calibration is recorded. Under the assumption of the typical Rayleigh scattering cross-section from literature, the relative and absolute calibration factors are estimated. While the in-situ Rayleigh relative calibration and the conventional relative calibration mostly agree within the error bars, the absolute calibration is too high by a factor of roughly 3. Variations between different scattering volumes need further investigation and probably make additional improvements of the setup necessary. However, the general suitability of the method as absolute calibration is confirmed.

Keywords: Detector alignment and calibration methods (lasers, sources, particle-beams); Plasma diagnostics - interferometry, spectroscopy and imaging; Data processing methods

*Corresponding author.
[1] See O. Grulke et al., *Nucl. Fusion* **64** (2024) 112002 for the full author list.

https://doi.org/10.1088/1748-0221/21/02/C02009

2026 JINST 21 C02009

Contents

1 Introduction

In nuclear fusion research, the Thomson scattering diagnostic is a widely used tool to determine electron plasma temperature and density by utilization of elastic scattering of electromagnetic radiation on individual charges (incoherent Thomson scattering) or correlated ensembles of charged particles (coherent Thomson scattering). Thomson scattering as a diagnostic has been applied in experimental plasma physics since the beginning of magnetic confinement experiments like the magnetic mirror experiment TMX [1], the T-3 tokamak [2] and the Princeton Model C stellarator [3]. As electrons are much lighter than ions, they are accelerated much easier in the external electric field of a laser pulse and act as main source for the dipole scattering [4], yielding orders of magnitude higher levels of scattered light than the ions. Therefore, in this paper the term of Thomson-scattered light is used to refer to the incoherent scattered laser light stemming from free plasma electrons.

To measure the plasma electron temperature and density, typically a pulsed, high-energetic laser is guided through the plasma. The Thomson scattering diagnostic now acts as a fast and super-sensitive spectroscopic measurement with an a-priori defined, deliberately limited resolution: the Nd:YAG laser pulses probe the charged particles within their own movement along the beam path. One or more (two in case of Wendelstein 7-X, W7-X) observation optics collect the scattered light from the intersection volume of the optics (fibers) lines-of-sight and the probe beam. A qualitative geometric overview about the scattering volumes, the Laser beam path and the lines-of-sight of the observation optics is given in figure 1.

As the laser spectrum undergoes a Doppler broadening and relativistic shift if the scattering particles (electrons) are moving relative to the observer, the scattered spectrum, under assumption of a relativistic Maxwellian electron velocity distribution, is unique for one temperature. An extensive discussion on the relativistic effects on the Thomson scattered spectrum can be found in [5, 6]. The collected light is split in only a few (five in case of W7-X) wavelength ranges, which are sufficient to determine the light distribution but not too many to ensure large, non-overlapping spectral bandwidths

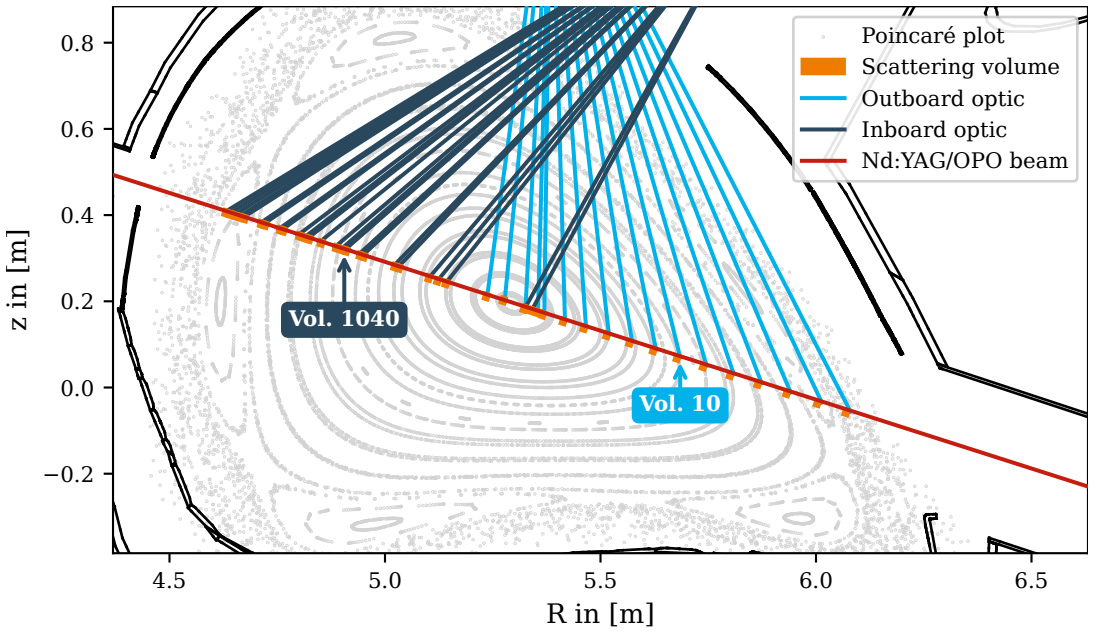

Figure 1. Cut through W7-X by the Thomson scattering plane (almost poloidal). The red line marks the laser-beam; the blue lines depict the routes of scattered light towards the inboard (of the torus) and outboard observation optics. The scattering volumes appear as orange squares with the two illustrative volumes highlighted. The Poincaré plot of the W7-X standard configuration and some vessel components are overlaid just for geometrical visualization purposes.

with a good signal-to-noise ratio in each wavelength-range (channel). The splitting is done by a cascade of band-pass interference filters and the integrated photon count is measured by Avalanche photodiodes (APDs) for each wavelength range [7]. The relative height of the signal levels between those channels yield the information about the electron temperature. The electron density can be determined as well, as an increased electron number inside the plasma results in a larger amount of scattered light.

Even if the TS diagnostic is providing data which is directly linked to the electron temperature and density, the data itself is useless without an appropriate calibration, considering all kinds of geometrical, physical and sensitivity related effects. At W7-X, for example, two calibrations are performed at the beginning and after each experimental campaign. One of those, the relative one, includes ideally the spectrally resolved transmission and conversion factors of all optical components between the scattering volume and the digitizer. The second one, the absolute calibration, uses the transmission information of the relative calibration and scales it to an absolute value. This means vividly that the information about the absolute scattering yield in a specific geometric location, and the relative spectral transmission are combined into a spectral set of values mirroring the absolute efficiency of photon detection and digitization for each scattering volume and each individual wavelength [8].

As mentioned above, the relative calibration should ideally include all the optical components of the TS diagnostic. At W7-X, the standard method for the relative calibration requires the retraction of the collection optics to place a scattering disc in front of them. Wavelength tunable, monochromatized light from an super-continuum laser is transported via an optical fiber into the torus hall and projected onto this disc, allowing a fine wavelength scan for all five optical channels (numbered according to ascending wavelength), including all of the retracted optics. However, as the scattering disc has to be

2026 JINST 21 C02009

placed in front of the observation optic, the plasma-facing vacuum window is not included in this calibration. But this window can be covered by re-deposition of particles released in plasma-wall-interactions, changing the transmission properties over time. Especially long discharges as targeted for W7-X and other large fusion experiments demonstrate the necessity of an in-situ calibration, without changes to the optical setup.

The current state-of-the-art absolute calibration at W7-X is using anti-Stokes-rotational Raman scattering of Nd:YAG laser pulses in nitrogen [8]. Here, one or two optical channels (of five in total), close to the laser wavelength can be absolutely calibrated, as the amount and spectral distribution (sharp Raman-lines) of the scattered light can be calculated analytically if the differential Raman-scattering cross-section is known [9]. The comparison of observed and calculated photon numbers yields the absolute calibration factor.

2 Rayleigh scattering as calibration method

Rayleigh scattering as (absolute) calibration method for Thomson scattering diagnostics has long been recognized by researchers [10] and is still applied in recent nuclear fusion experiments like NSTX [11] and LHD [12]. However, these Rayleigh scattering calibrations used a light source, sitting at a specific wavelength within one of the filters (typically a notch filter around the laser line just for this purpose) and the light obtained in this filter is used for the absolute scaling of the separately measured spectral calibration at this wavelength. With the rise of powerful pulsed, polarized and wavelength-tunable light sources like optical parametric oscillators (OPOs), the possibility was proposed to scan the entire wavelength range of all filters to combine the two measurements into a single calibration measurement [13, 14]. This method is in principle creating absolutely calibrated sensitivity functions for each wavelength. The pulse characteristic is important, since the TS diagnostic uses pulsed lasers in combination with APDs, which show a different transient behavior between short and long pulses/cw sources, making a comparison to the short-pulsed Thomson data impossible. The optical properties are also important: only if the scattering volumes, created by intersection of the path of the calibration and the observation optics lines-of-sight, have a similar size and location inside the vacuum vessel, the calibration yields meaningful values.

The expected time-integrated (over the pulse-width) Rayleigh signal s on the APD for a spectral channel i is described by [13]

$$\left(\int s dt\right)_i = \underbrace{b(\lambda)\cdot\varepsilon(\lambda)}_{:=\text{ Stray-light}} + \underbrace{n_{\text{gas}}\cdot\varepsilon(\lambda)\cdot\frac{d\sigma}{d\Omega}\cdot\frac{\lambda}{hc}\frac{g_i(\lambda)}{g_0}\cdot\delta L\delta\Omega g_0}_{:=\text{ Rayleigh scattered light}}. \tag{2.1}$$

It can be divided into a stray-light term and a Rayleigh scattered contribution. The Stray-light is defined by the wavelength-dependent pulse energy $\varepsilon(\lambda)$ multiplied with stray-light sensitivity factor $b(\lambda)$. Rayleigh scattering itself, similar to Thomson scattering, is elastic scattering of electromagnetic radiation on charges, which are accelerated in external electromagnetic fields and act as dipole oscillators. While for Thomson scattering the light is scattered on free (plasma) charges, Rayleigh scattering refers to scattering on bound electrons in atoms and molecules. The amount of Rayleigh scattered light is therefore dependent on the polarizability α of the atomic species and the orientation of the polarization. The Rayleigh scattered part is dependent on the gas (here: argon) particle number n_{gas},

2026 JINST 21 C02009

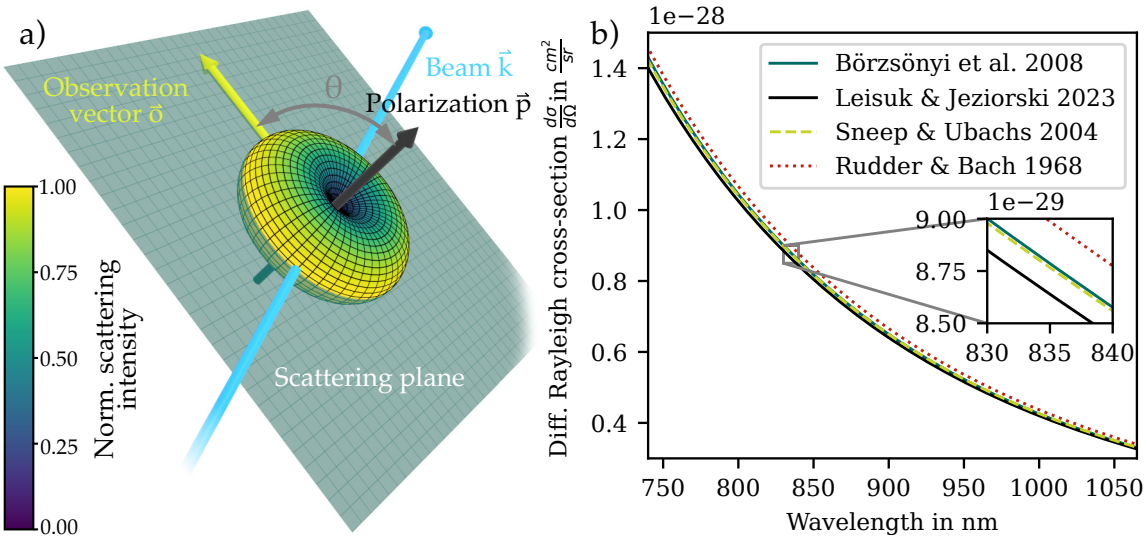

Figure 2. a) 3D plot of the normalized Rayleigh dipole scattering intensity with respect to it's polarization. The Observation vector $\vec{o}$ is pointing from the scattering particle to the observation optic, the beam $\vec{k}$ is pointing in the direction of the OPO beam and the polarization $\vec{p}$ is standing orthogonal on the scattering plane, defined by the first two. b) Calculated Rayleigh scattering cross-sections. For this work, the analytical expression for the dynamic polarizability and therefore the differential Rayleigh scattering cross-section in dark-green (Börzsönyi et al. 2008) is used, as it can be easily reproduced and is sitting in-between the extrapolated experimental values obtained with a SHG Nd:YAG (Sneep & Ubach 2005) and a ruby laser (Rudder & Bach 1964).

the pulse energy $\varepsilon(\lambda)$, the differential scattering cross-section $d\sigma/d\Omega$, the photon-number normalized *relative spectral calibration factor / sensitivity* $g_i(\lambda)/g_0$ and the *absolute calibration factor* $\delta L \delta\Omega g_0$, taking into account the geometrical length δL of the scattering volume, the observation angle $\delta\Omega$ and the absolute quantum efficiency of the APD of the volume's reference channel g_0 [13]. The differential cross-section used in this work is obtained as described in [15] using

$$\frac{d\sigma}{d\Omega}(\lambda) = \frac{\pi^2 \alpha^2(\lambda)}{\varepsilon_0^2 \lambda^4} \sin^2(\theta)\,, \tag{2.2}$$

with the theoretical dynamic polarizability $\alpha(\lambda)$ calculated via the Lorentz-Lorenz eq. and the refractive index. For the refractive index, the coefficients for the Sellmeier-eq. from [16] are used. Equation (2.2) is only valid, if the light is linearly polarized. In the case of the W7-X Thomson scattering system, the polarization is fine-tuned by a half-wave-plate (HWP) to stay orthogonal to the scattering plane, resulting in $\theta \approx 90°$ for all scattering volumes. The orientation of the scattering plane and the normalized scattered fraction (parameterized in 3D as in [17]) are shown in figure 2 a). As comparison, eq. (2.2) is also used in combination with the static polarizability for argon, found in [18] in the static limit. These cross-sections are compared in figure 2 b) with the experimental values found in [19] for 532.2 nm (SHG Nd:YAG) and in [20] for 694.3 nm (ruby laser), both processed and extrapolated in the way described in [11].

Optical parametric oscillators are nothing new [21–23] but became relevant only with powerful pump-lasers. They contain a pump source (typically a frequency doubled or tripled Nd:YAG laser) in combination with a second stage — the actual optical parametric oscillator. The biggest advantage of an OPO is its tunability: the resonant wavelength inside the cavity and therefore the difference

2026 JINST 21 C02009

between pump and idler can be tuned by turning the crystals and changing the wavelength accepted for critical phase-matching and as a result, the signal wavelength. Previous experiments showed promising proof-of-principles of spectral and absolute calibrations. However, the measurements suffered from a low signal-to-noise ratio which is a major drawback of this technique: as the gas atoms are at room temperature, almost no spectral broadening or shifting of the incident laser wavelength can be observed and the scattered light is always sitting at the same wavelength as the incident beam — a source for in-vessel stray light contamination. The pure Rayleigh signals in those measurements were often smaller than 50% of the total signal, even if the plasma-facing windows, which are expected to be the main sources for stray-light, were Brewster-angled (as for W7-X) and atmospheric pressures were used [14].

3 Experimental setup

The design of the Thomson scattering system at W7-X itself is presented in [7, 8]. The path of the scattered signal from its source to its acquisition and digitization is important for this work, which is why it is briefly summarized here: assuming a plasma vessel filled with some kind of scattering media (gas or plasma): then light from the OPO or the Nd:YAG lasers will be scattered along the beam path. The fictional scattering volume is the volume, in which the laser beam has to lie in order for the detected amount of scattered light to be maximum. The size of a scattering volume is determined by the transfer function of the lens-stack of the particular optic, the numerical aperture of the fibers and the distance between the laser beam path and the optic.

The intersection between the scattering volume and the laser beam acts as volumetric light source during the measurements, in which light is scattered as shown in figure 2 a). A part of the scattered intensity is matching the acceptance angle of a fiber within one of the optics. Before reaching the optic, the light has to pass-through the plasma-facing window sitting at the bottom of the optics's immersion tube inside the cryostat. The water-cooled window shields the volume of the plasma vessel from the surrounding air. Both observation optics together contain several optical multi-mode fibers sitting behind a focusing lens stack, from which currently 42 are connected to polychromators. A correspondingly large number of usable scattering volumes exists at absolute positions inside the plasma vessel. The beam path of the OPO laser (which is approximately the same as for the Nd:YAG's) is shown in figure 1.

A polychromator is a box which contains an achromatic lens, collimating the light passing through the connected fibers and multiple optical interference band-pass filters. Only a specific optical bandwidth is passing through the filters, reaching the avalanche photo-diodes (APDs), while the rest of the spectrum is reflected onto the next filter. Currently, the system consists of a combination of five interference filters with avalanche photodiodes. By using optical fibers of different lengths ("delay lines"), each polychromator can observe the spectra for two (or in some cases three) scattering volumes.

Many points affect the transmission properties for each individual scattering volume differently, such as: each fiber has their own damping coefficient; the filters are not perfectly identical in each polychromator due to manufacturing imperfections; the avalanche photodiodes have different sensitivity functions; the beam illumination of the scattering volumes can deviate at certain positions and the plasma facing window can be coated anisotropically. Consequently, the calibration for the combined components has to be performed for each scattering volume and temporally as close as possible to the Thomson scattering measurement (e.g. shortly before or after the experimental campaign).

2026 JINST 21 C02009

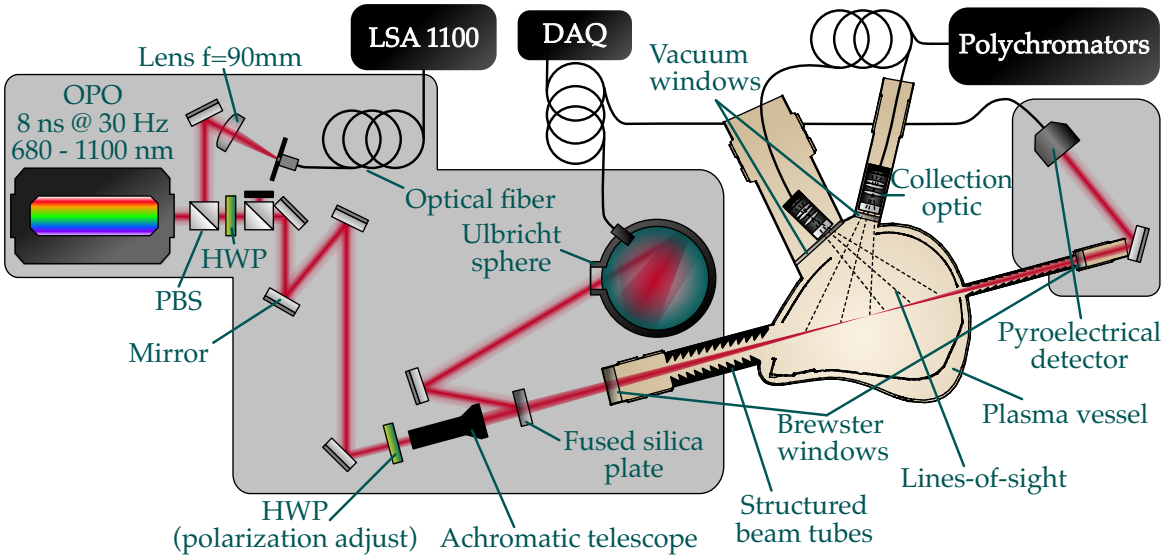

Figure 3. OPO beam path with all relevant optical components for Rayleigh scattering inside the vacuum vessel (not to scale). The abbreviations HWP and PBS stand for half-wave plate and polarizing beam splitter.

The specific beam path as shown in figure 3 for the Rayleigh scattering measurement was build on the basis of the one described in [14]. To decrease the mentioned amount of stray light during the measurements, the beam guiding tubes were re-made from fine-structured metal, which is reflecting light only out of the vessel. The beam with the old focusing lens ($f \approx 5$ m) setup was so divergent, that parts of the beam were cut by the guiding tube at the OPO beam exit, eventually leading to a large stray-light contribution and rendering the absolute energy measurement inaccurate. To overcome this issue, an achromatic zoom telescope (Thorlabs ZBEB2) was chosen to replace the old lens in order to decrease the beam divergence by beam magnification (using a factor of two) at the entrance. In combination with a focusing distance of approximately 6 m this lead to an effective focal length (effective as in combination with the OPO's beam divergence) of approximately 8.5 m, resulting in a more consistent beam size within the plasma vessel. The beam diameter at the entrance and exit of the vacuum vessel is now smaller than the size of the scattering volume (ca. 7–40 mm in the observation plane) and was not cut anywhere, allowing the calculation of the Rayleigh scattered light by using the entire energy measured with the pyroelectrical detector PEM45K from SLT Sensor- und Lasertechnik GmbH.

Additionally, a second energy measurement, independent of the beam position was added. This measurement uses an Ulbricht sphere which is connected to an InGaAs photodiode via multiple optical fibers. As small vibrations of the setup affect the beam pointing especially over large distances, the Ulbricht sphere is an elegant counter-measure: as long as the beam is hitting the opening hole of the Ulbricht sphere, the rough inner surface of the sphere is scattering the light diffusely, and the light distribution inside the sphere becomes almost homogeneously. The amount of light reaching the fibers and the photodiode becomes independent of the exact position of the beam.

The heart of the Rayleigh measurement is the optical parametric oscillator Innolas SpitLight OPO 1000 with a pulse-width of approximately 8 ns, a tuning range of 680–1100 nm (pumped at 532 nm, SHG of Nd:YAG) and an improved repetition rate of 30 Hz compared to previous measurements [14].

2026 JINST 21 C02009

The beam shape close to the laser head looks cross-like but becomes almost circular after focusing. To guide the OPO beam, broadband dielectric mirrors from Newport (20Q620BB.HR2) and angle-optimized ones from Laseroptik were used. At high pulse energies, the amount of stray-light is already sufficient to saturate the APDs completely, making a Rayleigh measurement impossible and therefore an energy attenuation mandatory. To reduce the pulse energy to the low levels needed for the Rayleigh measurement, two stacked polarizing beam splitting cubes (Thorlabs PBS 255) are used in combination with an achromatic half-wave plate (Thorlabs AHWP10M-980) in a typical polarizer-HWP-analyzator setup. The first one ensures the existence of only one polarization at the HWP in a rotation mount which is used with a second PBS to reduce the energy. A positive side-effect is the determination of the polarization by this setup. This ensures, that no unwanted polarizations are reflected on the Brewster-angled windows to the vacuum vessel — probably leading to additional stray-light. Additionally, the internal amplifier delay of the OPO's pump laser is used to fine-tune the output pulse energy of the OPO between measurements without requiring any physical manipulation of the system. However, too high amplifier delays result in unstable output energies, limiting the fine tuning to a factor of two or three.

The unmatched and therefore reflected polarized light from the first PBS is guided through a $f = 90\,\mathrm{mm}$ lens to a optical single mode fiber which is connected to the grating-based laser spectrum analyzer LSA 1100 from HighFinesse GmbH. The spectrum analyzer measures the central wavelength and the spectral width of the OPO output beam during the Rayleigh calibration with an automatic exposure time between 30 µs and 3 s to ensure at least one measurement for each selected wavelength.

4 Measurements

All measured diode signals (InGaAs photodiode after the Ulbricht sphere and the different APDs inside the polychromators) are processed in the following way: the time integral of the measured voltage peak with subtracted mean of the noise floor is proportional to the number of the photon counts (eq. (2.1)). To obtain the boundaries of this integral for one spectral channel, the diode signal was summed over the following 100 periods, peaks were searched and the boundaries were defined by fixed bounds around those peaks. The repeated verification of the integral bounds during the analysis is necessary, as the exact position in the stored time frame varies between the different spectral channels and for each polychromator.

The serial output of the OPO's control software is used to store the internal energy measurement of the OPO, additionally to the time-step, the set-point-wavelength and the number of OPO pulses per wavelength. This internally recorded data is utilized to map the wavelengths to the data recorded by the main DAQ. The mapped data is grouped by the wavelength and the mean and it's standard deviation are calculated for each group / wavelength. In the following, we only refer to these mean values and use them instead of the single-pulse values.

According to eq. (2.1), the integrated polychromator signal for a scattering event is dependent on the energy of this pulse. To obtain the sensitivity of the diagnostic, the mean polychromator signal is divided by either the energy measurement of the pyroelectrical detector or the relative signal recorded by the Ulbricht sphere diode which can be linearly scaled to the absolute PEM energy measurement. The energy measurement was split into two intervals, as the InGaAs photodiode has a strong wavelength dependency, which leads to a strongly decreased photon efficiency at high wavelengths. Also, the efficiency of the parametric amplification inside the OPO has it's maximum around 800 nm. Both

2026 JINST 21 C02009

curves can be found in figure 2 b). Additionally, the channels 3–5 of the polychromators get less sensitive with increasing wavelength, as the sensitivity of the avalanche photodiodes is also reduced there. To get a good signal above the electronic noise of the amplifiers, different energies were chosen for the two wavelength ranges, split between 1018 and 1020 nm. The ideal measurement would have been split into two wavelength ranges for both observation optics individually, as the stray light saturates both optics differently. However, since the experimental time was limited, two different energy steps (one for the inboard and one for the outboard optic) in the lower wavelength range 740–1018 nm and one for both in the high wavelength 1020–1065 nm range were chosen.

The wavelengths used for the analysis were set closer to each other in the expected locations of the filter edges, leading to an increased resolution in these areas. For the low-wavelength range, a coarse $\Delta\lambda$ of 2.0 nm and a fine $\Delta\lambda$ of 0.2 nm was used. The resolutions in the high wavelength range above 1020 nm was chosen to 2.0 nm and 0.1 nm respectively. While for the Thomson scattering diagnostic, the coarse resolution is sufficient (the spectral distribution function of the TS scattered spectrum has only small gradients), the high resolution is in fact needed only for scaling of any relative calibration to the absolute calibration done by the conventional Raman scattering method. The absolute calibration factor there is determined by using the relative calibration in combination with the calculated Raman line spectrum, to see which fraction of the Anti-Stokes-Raman lines is sitting in the spectral channels 4 or 5 (close to the laser wavelength). Small deviations of the measured filter edge locations can lead to large errors in the absolute scaling factor. Therefore, a 0.1 nm resolution was chosen for wavelengths above 1018 nm.

The used OPO calculates the absolute crystal position for critical phase-matching by using a polynomial calibration file. That means that the set-point wavelengths do not necessarily correspond exactly with the emitted wavelength. In cooperation with the OPO manufacturer Innolas Laser GmbH, and online-tracking of the real output wavelength and pulse width utilizing the laser spectrum analyzer LSA 1100 was developed. Using these wavelengths, the measured calibration curves can be interpolated on a fixed wavelength grid to make the different measurements comparable.

4.1 Stray light measurement

Rayleigh scattering occurs at the wavelength of the incident light. That means that if one wants to use Rayleigh scattering to determine the spectral sensitivity of an optical system, the light source has to cover the entire wavelength range. That also means that any kind of stray light, occurring for example from Fresnel reflections on the Brewster windows if the beam is not entirely p-polarized with respect to the window surface, will be directly visible on the highly sensitive photodiodes. Other possible stray-light origins are for example the straying on the plasma-coated layer on the vacuum windows as mentioned in section 3 or light cut and reflected somewhere (e.g. at mirror-corners or limiting apertures) along the beam path (figure 3). This is problematic, as the intensity of Rayleigh scattered light is typically around 10 orders of magnitude lower than the beam intensity itself ($\propto \lambda^{-4}$). Even though W7-X is a carbon machine, large parts are made from stainless steel, especially the port surrounding the plasma facing window. Stray light scattered in the ports is one of the largest problems using Rayleigh scattering and has to be reduced as much as possible in order to get a good signal-to-noise ratio. The Rayleigh contribution of the total signal is obtained by subtracting a dedicated vacuum background measurement characterizing the stray-light contribution.

2026 JINST 21 C02009

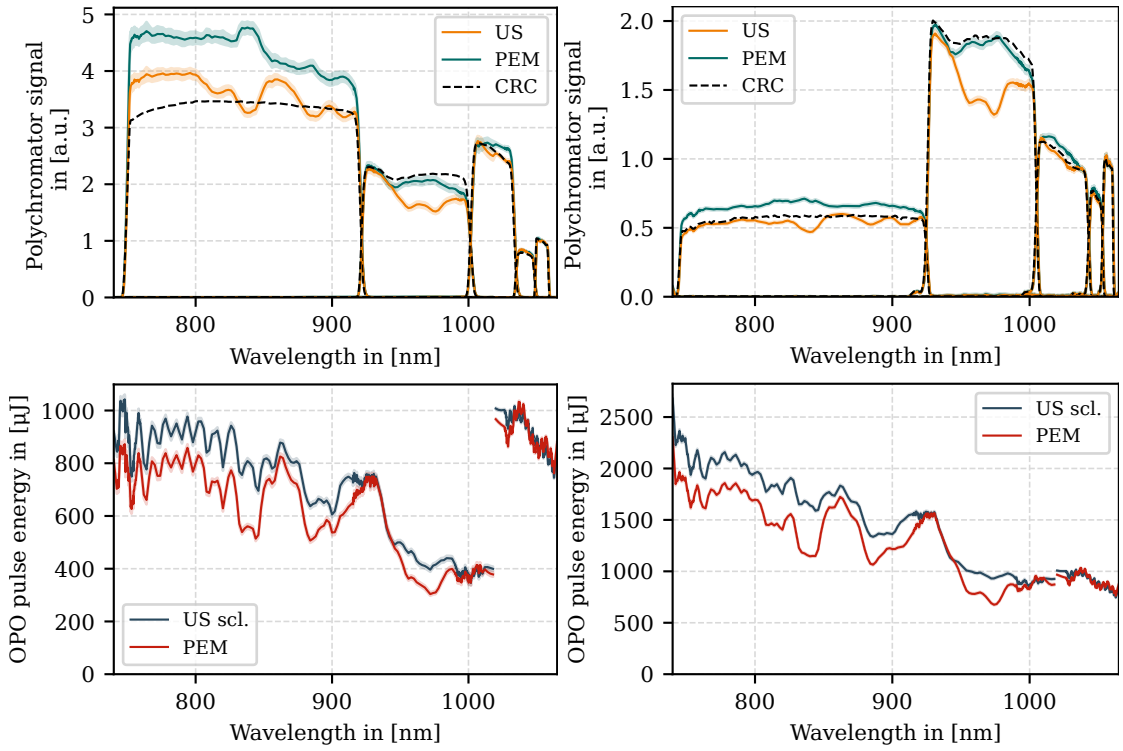

Figure 4. Stray light measurement for scattering volume 10 (left) and volume 1040 (right), normalized to the energy of the OPO pulses (either by the pyroelectrical detector, PEM or the PEM scaled Ulbricht sphere diode measurement, US) shown in the lower plots. The result is normalized to the energy-related signal at 1054.0 (left) or 1055.0 nm (right). As comparison, the conventional relative calibration (CRC) is overlaid as well. The shaded area represents the 2-σ standard error of the mean.

The stray light measurement for this paper was repeated two times — once before and once after the argon measurement, while the time between the second vacuum measurement and the argon measurement was much smaller (several hours instead of days) than for the first one. Therefore, the second vacuum measurement is used as reference in this paper. The consistency with the first vacuum measurement was checked nevertheless. The obtained sensitivity curve for the stray light vacuum measurement can be found in figure 4 for two different scattering volumes. The five separated curves belong to the five spectral channels of one polychromator. The lower graph shows the energy measurement to which the polychromator signal is normalized. As mentioned in the introduction of section 4, the energy scan is divided into two wavelength ranges to obtain satisfactory signal-to-noise ratios for the less sensitive filters (channel 4 and 5). This manifests in a jump in the energy between 1018 and 1020 nm. The normalized polychromator signal is not showing this jump, indicating, that the normalization works as intended.

The energy measured by the pyroelectrical detector (PEM45K) and the absolutely scaled Ulbricht sphere energy measurement show approximately the same slope, but are of course not of the same height on each point. That is not surprising, as the linear scaling was evaluated at only one wavelength (900 nm) and then scaled by the provided spectral quantum efficiency of the InGaAs photodiode. Therefore, part of the discrepancy could be that the Ulbricht sphere photodiode has a sensitivity curve, not matching the ideal curve provided by the manufacturer. Also, the coating of the Ulbricht sphere

2026 JINST 21 C02009

and the optical fibers for the light transmission between Ulbricht sphere and InGaAs photodiode can impinge some wavelength dependent effects, not yet considered. In general, there are three areas visible, where the two measured energies deviate the most, leading to strong variations in the normalized signal. Interestingly, several features visible in all of the scattering volumes (e.g. around 850 nm) seem to be anti-correlated between the two energy measurements. One possible explanation is that parts of the beam energy are lost at the two plasma-facing Brewster windows (entrance and exit to the vacuum vessel). Hence, the Ulbricht sphere (before the first window) may over- and the pyroelectrical detector (after the second window) underestimate the beam energy inside the vessel. If this assumption holds, one possible approach in the future would be to estimate the beam energy inside the vessel by averaging the two measurements. In this paper, however, we are using both energies separately, since a confirmation of this hypothesis is work in progress.

In principle, the stray light measurement alone already reveals parts of the calibration's information [24]. This information is masked by the fact, that the optical spectrum of the stray-light is not fully known: scattering on coated or generally different materials inside the plasma vessel can lead to wavelength dependencies in the "stray-light-source-spectrum", that can vary in principle for each observation cone. Because of that reason, the stray light measurement is probably not ideally suited as a stand-alone measurement; but as it only requires an evacuated machine and remote access, this is one of the easiest and repeatable measurements even at large fusion experiments and could be used as a quick health check of the diagnostic during the experimental campaign [24]. In figure 4, the two differently normalized polychromator signals are compared to the current reference calibration using a super-continuum light source.

4.2 Argon measurement

Argon is the cheapest option for atomic Rayleigh scattering without any Raman contributions, typically occurring in molecular gases. The amount of expected Rayleigh scattered light can be calculated by knowledge of the differential scattering cross-section of argon. This fraction is typically masked by the stray-light measured in the previous section. For this calculation it was assumed that the observation of the scattered light occurs exclusively in the observation plane shown in figure 2 a) for all scattering volumes and all wavelengths.

The intensity of the scattered light scales indeed linearly with the amount of argon atoms inside the scattering volume. This can be shown by starting at a high pressure (377 mbar in our case) and reducing the pressure inside the plasma vessel step-wise. The scaling of the energy-normalized signal in each scattering volume depends on the exact spectral sensitivity of the corresponding spectral channel at the measurement wavelength and is therefore volume-specific. The linear scaling for two scattering volumes can be found in figure 5, obtained for a limited number of wavelength values.

The data acquisition for the entire spectral range was performed at an argon pressure of approx. 377 mbar inside the plasma vessel. The energy normalized argon measurement is shown in figure 6 for two scattering volumes — one in each collection optic. In contrast to the stray-light measurement, the energy dependent dips are less obvious for the argon measurement normalized to the PEM. However, this seems not to be the case for the signal normalized to the Ulbricht sphere.

2026 JINST 21 C02009

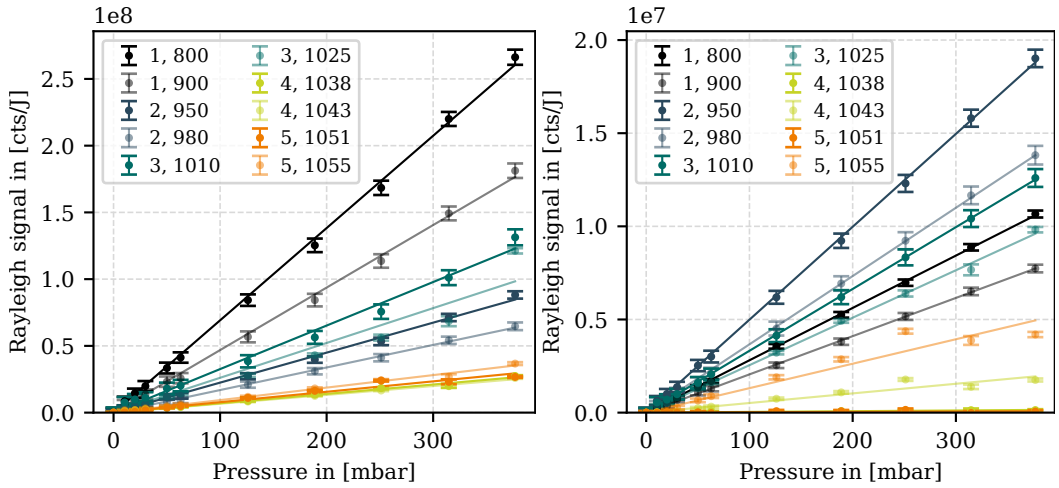

Figure 5. Energy-normalized Rayleigh signals for volume 10 (left) and volume 1040 (right) at different argon pressures. The stray-light background has been subtracted. For each channel (first number in the legend), the pressure scaling for two wavelengths was measured (second number). The linear scaling deviates for the two scattering volumes. The error bars denote the 2-σ confidence interval of the mean. Each data point corresponds to the average over 1000 samples.

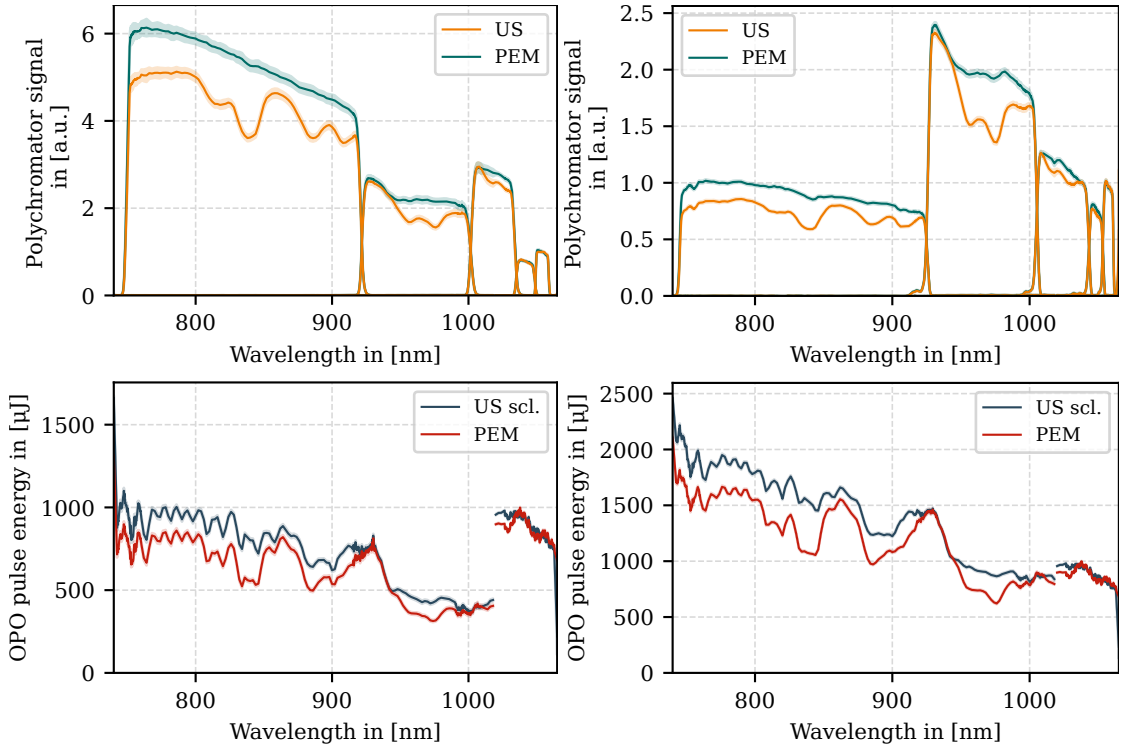

Figure 6. Energy-normalized polychromator signals for volume 10 (left) and volume 1040 (right) in 377 mbar argon with the corresponding energy measurement. The Rayleigh signal is masked by the in-vessel stray light. Besides the different normalizations of the polychromator signals, the 2-σ confidence interval of the standard error of the mean is shown.

2026 JINST 21 C02009

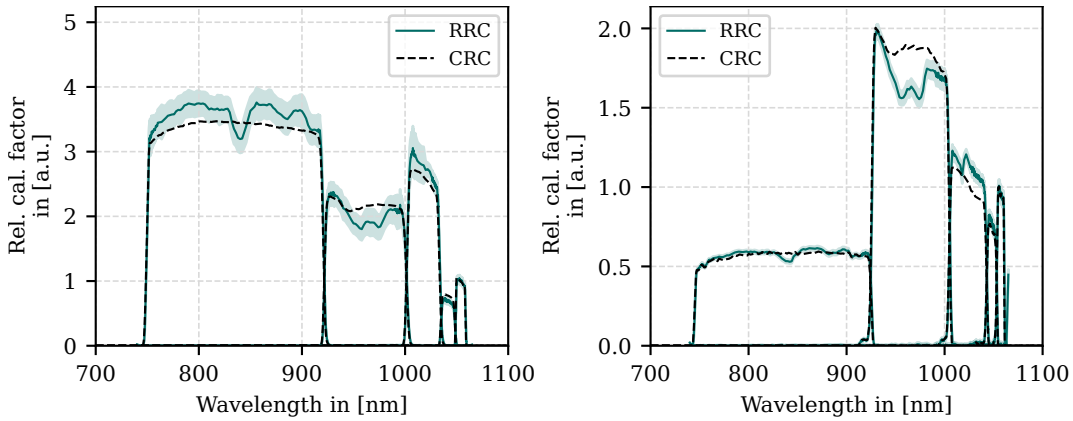

Figure 7. In-situ Rayleigh relative calibration (RRC, sensitivity function) of scattering volume 10 (left) and volume 1040 (right), normalized to the sensitivity at 1054.0 (left) and 1055.0 nm (right) nm in spectral channel 5. The black dotted line corresponds to the conventional ex-situ relative calibration method using the super-continuum laser (super-k).

4.3 Relative calibration

The relative calibration g_i/g_0 is determined by the difference between the energy-normalized signal measured in 377 mbar argon and the stray-light signal from the vacuum measurement, divided by the differential Rayleigh scattering cross-section, the conversion factor and the electron number density (compare eq. (2.1)). The results for the previously considered volumes can be found in figure 7. In this figure, the relative calibration is also compared to the one measured by the super-continuum laser. Even if the PEM-normalized values are used, the signal is showing huge variations in the same areas as in the argon and the stray-light measurement. Here, a disadvantage of the Rayleigh scattering method becomes visible: the splitting into two independent measurements is prone to inconsistencies between them, like small changes in the energy, beam pointing and output wavelength (in combination with an forward controlled OPO laser, without a wavelength feedback). The Rayleigh signal is just a small fraction of the total signal and this results in noisy sensitivity curves. The semi-transparent area is marking the 2-σ confidence interval around each signal.

It can be seen that the two calibrations agree mostly — at least within the relatively high error bar of the in-situ method.

4.4 Absolute calibration

In the case of the Rayleigh calibration, the absolute calibration $\delta L \delta \Omega g_0$ can be directly obtained from the difference between the normalized vacuum and argon signal, rearranging eq. (2.1). The normalization to a specific wavelength becomes obsolete as this calibration method is in principle returning absolute calibration factors for each measurement wavelength independently from each other.

Ideally, the absolute calibration factors determined by this method should resemble the ones obtained from Anti-stokes-rotational Raman scattering in nitrogen for the same scattering volume. The comparison can be found in figure 8 for the previously mentioned scattering volumes. The green line represents the Rayleigh absolute calibration (RAC) utilizing the OPO and the Rayleigh cross-section scaled, energy-normalized difference between the signals in 377 mbar argon and vacuum. The desaturated region corresponds to the 2-σ confidence interval of the mean. Additionally, the

2026 JINST 21 C02009

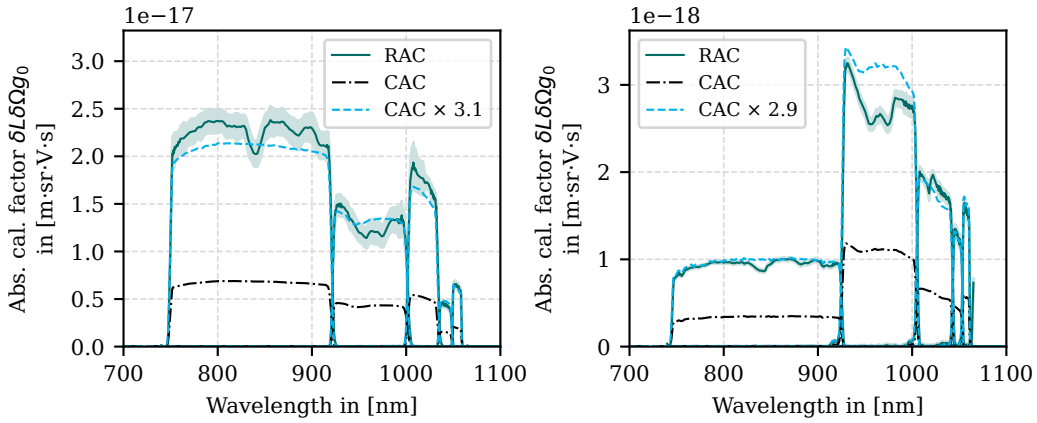

Figure 8. Absolute calibration factor obtained by the In-situ Rayleigh OPO measurement (RAC, green) in comparison with the conventional absolute calibration (CAC): the CRC scaled by the factor obtained by the Anti-Stokes-Raman measurement in spectral channel 5 (black). The blue curve corresponds to the scaling factor determined by a channel-square-weighted LMSQ-fit of the CAC to match the in-situ calibration (RAC).

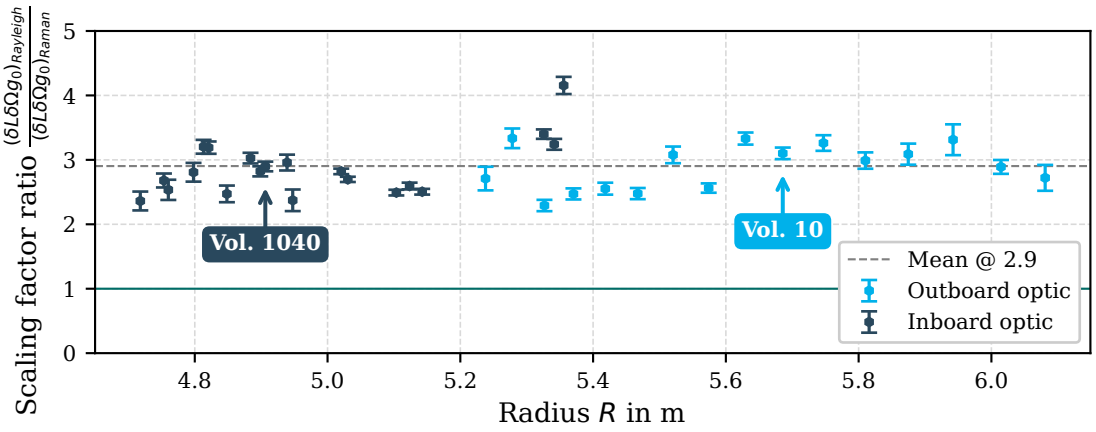

Figure 9. Scaling factor ratios between the Rayleigh absolute calibration and the Raman absolute calibration obtained by the method described for figure 8, plotted over the absolute radial position of the scattering volume in the torus hall coordinate system. Two colors are used to distinguish between the two observation optics. The ideal value of one is marked as horizontal line, as well as the mean for most scattering volumes, excluding volumes. The bars mark the 2-σ confidence interval of the mean.

black dash-dotted line depicts the conventional absolute calibration (CAC), obtained by scaling of the conventional relative calibration (CRC) by the factor determined from the Anti-Stokes Raman scattering measurement in nitrogen. To identify the ratio between both calibration methods the CAC was scaled by a factor within a LMSQ-fit routine to match the RAC. The relative and absolute spectral calibrations for all scattering volumes can be found in appendix A to illustrate that every single volume could be calibrated by this method. This had not been possible before due to prohibitive levels of stray-light.

Figure 9 shows the scaling of the absolute calibration factor ratio between the Raman-scaled relative calibration and the Rayleigh absolute calibration for the two observation optics and radial position in the torus hall reference coordinate system. As the deviations in the shape of the sensitivity

2026 JINST 21 C02009

functions are limited to spectral channels 1 and 2, they are not influencing the absolute scaling as this is evaluated with a strong weight in favor of channels 4 and 5.

Two deviations can be observed: firstly, there is a constant factor between the calibration factors of the two methods and secondly a considerable scatter around this value is found.

The absolute scaling is strongly dependent on the energy scaling. The most precise energy measurement is expected for the OPO Rayleigh measurement, as here the energy of the beam is measured directly after leaving the plasma vessel. This is not possible for the much more powerful Nd:YAG lasers used for the Raman- and Thomson scattering measurements, as their pulse energy and time-integrated thermal load is too high for the pyroelectrical detectors. Therefore, just a small fraction is coupled out onto the PEMs. This means that for those measurements, an out-coupling factor must be determined experimentally for each calibration, which directly influences the absolute scaling factor. The density determined by the Thomson scattering system is not affected by any absolute error in the energy measurement, since the same error occurs in the energy measurement during the Raman calibration and Thomson scattering measurement. But if the absolute calibration is determined independently, the incorrect energy measurement leads to an scaling factor between the two calibrations. An independent verification of the beam energy of the Nd:YAG laser is planned for the near future.

The scattering of the absolute scaling factors around a mean value on the other hand indicates experimental errors not yet accounted for. In principle, these can arise from either one of the two calibrations and require further analysis. One possible contribution is beam-misalignment since the two lasers do not share the exact beam path, but also the statistical errors of both calibrations have to be considered. Note that the error bar in figure 9 only represents the statistical error of the Rayleigh measurement but ignores the possibility that also the Raman reference could be incorrect.

Overall, the observed scatter seems too large for replacing the current standard approach of using Raman scattering for the absolute calibration. Nevertheless, with further improvements it seems possible to either replace or supplement the Raman calibration.

5 Discussion

This work intended to prove the suitability of the in-situ Rayleigh calibration as a method for the relative and absolute calibration of all scattering volumes at Wendelstein 7-X. In the frame of the Rayleigh calibration two independent measurements were carried out. A background stray light measurement without any gas, which already gives a rough estimate of the relative channel heights and therefore the spectral calibration, and another measurement with an argon flooded plasma vessel. From the difference between both energy-normalized measurements the Rayleigh scattered signal was obtained. This led to the reconstruction of the relative and absolute sensitivity (calibration) considering the wavelength dependent differential cross-section of Rayleigh scattering.

The relative calibration using the Rayleigh scattering method showed a satisfactory agreement with the standard calibration utilizing the super-continuum light source within the error bars. However, some features were observable in certain wavelength ranges for all scattering volumes indicating possible inconsistencies in the energy measurement and possible losses at the entrance and exit-window of the plasma vessel. Further improvements of the experimental setup are required to account for this.

Concerning the absolute calibration, a constant deviation from the Raman reference was observed. This deviation could possibly be caused by an inconsistent absolute energy scale between the Rayleigh calibration and the Nd:YAG lasers used for Thomson scattering. However, this remains to be verified.

2026 JINST 21 C02009

Additionally, apart from this constant deviation, a substantial scatter was observed when comparing the Rayleigh to the Raman calibration for the different scattering volumes. This scatter indicates the need for further improvements of the experimental setup to reduce statistical errors and ensure nearly identical beam paths for the Nd:YAG and the OPO lasers.

Nevertheless, the presented results demonstrate a substantial step forward in establishing Rayleigh scattering as a method for a combined in-situ relative and absolute calibration for Thomson scattering diagnostics as envisioned in [13] and [14]. With the improvements outlined in this contribution to reduce the impact of stray-light on the measurement it was possible for the first time to calibrate all 42 scattering volumes of the W7-X Thomson scattering diagnostic with this calibration method. To overcome the remaining issues, a detailed characterization of the laser window transmission is required as well as an independent confirmation of the absolute energy measurement of the Thomson scattering diagnostic.

Acknowledgments

This work has been carried out within the framework of the EUROfusion Consortium, funded by the European Union via the Euratom Research and Training Program (Grant Agreement No. 101052200 - EUROfusion). Views and opinions expressed are however those of the author(s) only and do not necessarily reflect those of the European Union or the European Commission. Neither the European Union nor the European Commission can be held responsible for them.

A Measured absolute calibrations for all scattering volumes at W7-X

With the new measurement setup in this paper, calibration measurements for all scattering volumes at Wendelstein 7-X could be recorded for the first time. Overview plots of the absolute calibrations can be found in figure 10. A larger deviation in the slope of the curves can be found for volumes 13–16 which is owed to an additional low-pass (frequency) filter during the measurements. This filter is only affecting channels 1 and 2 completely and channel 3 partially and was not included in the black reference calibration. Channel 4 and 5 agree quite well with the reference if the formerly found scaling is applied (blue dotted line).

The discrepancy in volumes 1067–1076 most likely belong to a different scaling of those channels (close to the outer plasma edge) in the current reference calibration and at this point it is not clear, which one is more accurate. However, even if the ratio between both absolute calibration methods is rather large for these volumes, the relative calibrations (the scaling between the channels) look reasonable if enough signal was measurable in channel 5. As typical for volumes close to the ports, the signal-to-noise ratio of the Rayleigh calibrations is reduced. Further improvements of the setup are needed to overcome the issues for those volumes.

2026 JINST 21 C02009

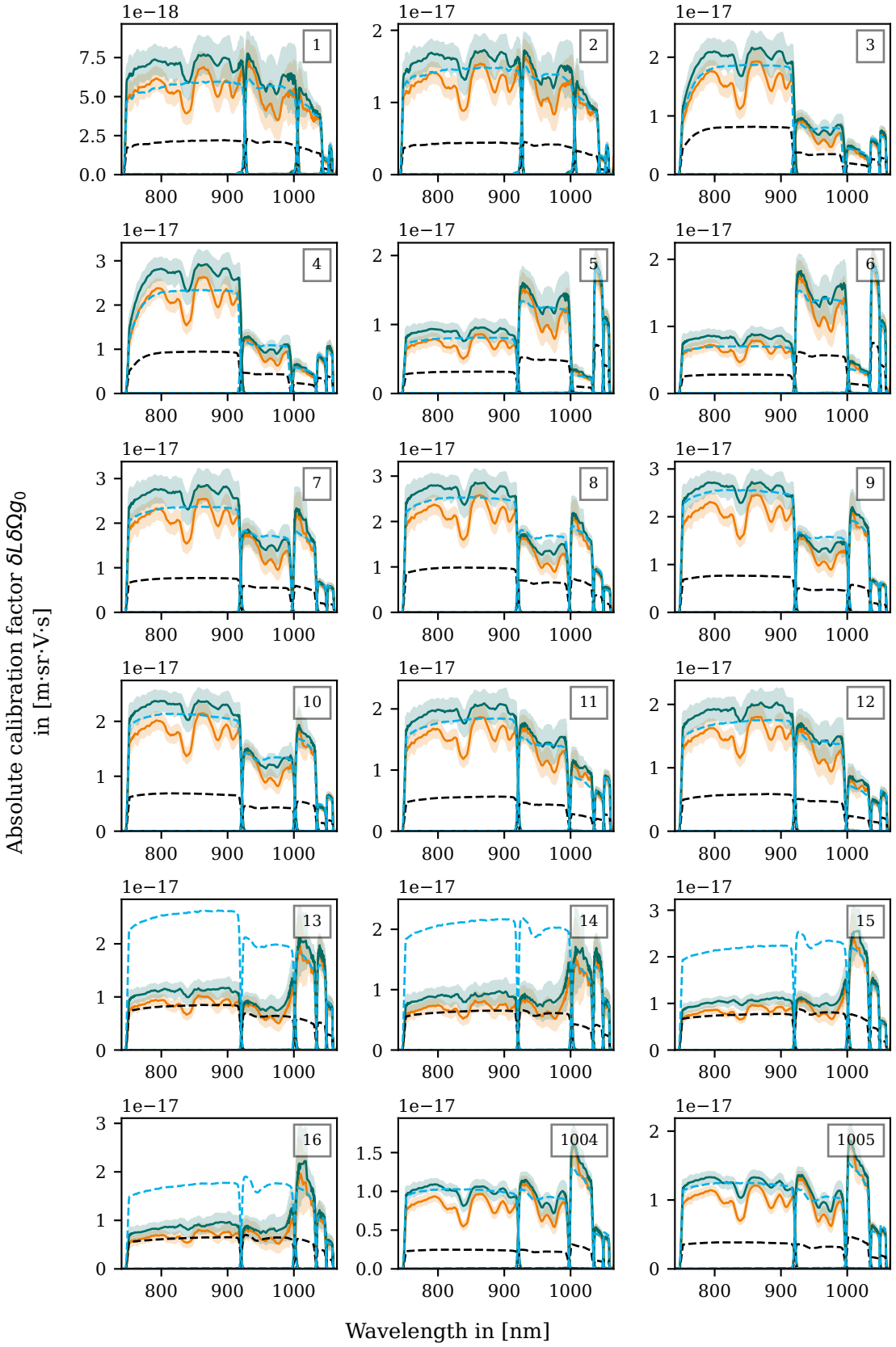

Figure 10. Continued on the next page.

2026 JINST 21 C02009

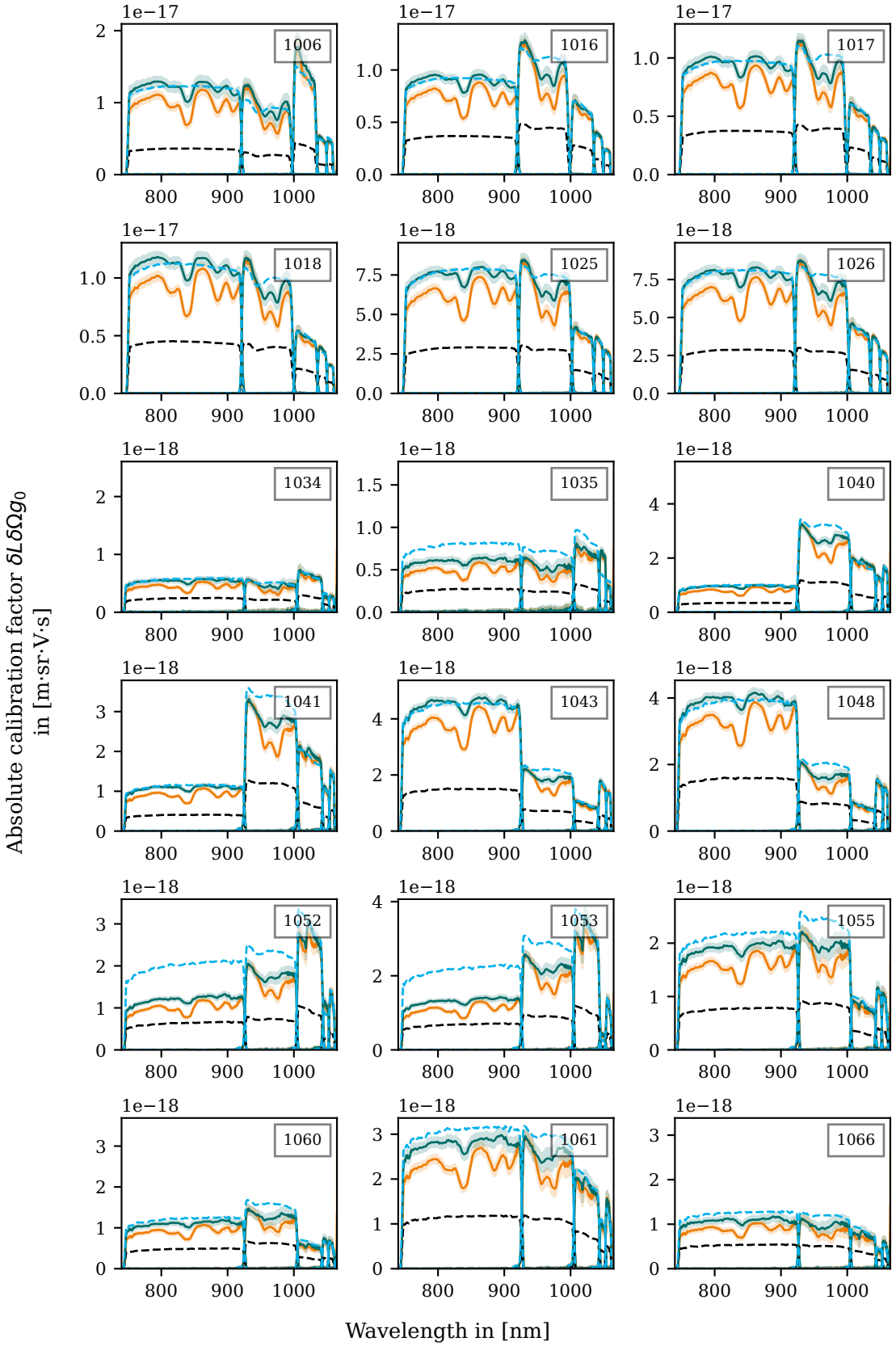

Figure 10. Continued on the next page.

2026 JINST 21 C02009

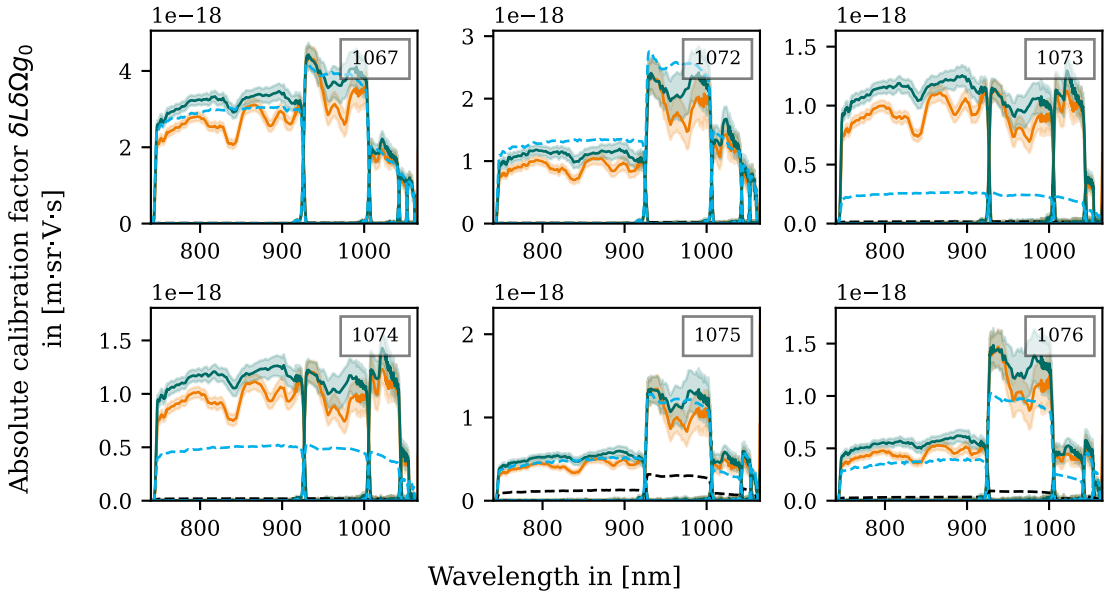

Figure 10. Absolute calibrations obtained by the OPO Rayleigh measurement normalized to the PEM measured energy (green) and the scaled Ulbricht sphere diode measured energy (orange), compared with the reference relative calibration scaled by the Raman factor (black) obtained for spectral channel 5. The blue dotted line corresponds to the fit between the reference absolute calibration and the Rayleigh calibration, yielding the scaling factor shown in figure 9. The numbers inside the boxes refer to the internal volume numbers — numbers up to 16 are collected by the outboard optic and the others by the inboard optic. Volumes 13–16 show a larger discrepancy in the first two channels due to an external filter applied in the vacuum measurement to avoid overexposure in these volumes.

References

[1] R.K. Goodman et al., *Thomson-scattering systems on TMX*, Tech. Rep. Lawrence Livermore National Laboratory (LLNL) (1982) [DOI:10.2172/5259125].

[2] N.J. Peacock et al., *Measurement of the Electron Temperature by Thomson Scattering in Tokamak T3*, *Nature* **224** (1969) 488.

[3] S. Yoshikawa and T.H. Stix, *Experiments on the Model C stellarator*, *Nucl. Fusion* **25** (1985) 1275.

[4] I.H. Hutchinson, *Principles of Plasma Diagnostics*, Cambridge University Press (2002) [DOI:10.1017/cbo9780511613630].

[5] O. Naito, H. Yoshida and T. Matoba, *Analytic formula for fully relativistic Thomson scattering spectrum*, *Phys. Fluids B* **5** (1993) 4256.

[6] S.L. Prunty, *A primer on the theory of Thomson scattering for high-temperature fusion plasmas*, *Phys. Scripta* **89** (2014) 128001.

[7] E. Pasch et al., *The Thomson scattering system at Wendelstein 7-X*, *Rev. Sci. Instrum.* **87** (2016) 11E729.

[8] S.A. Bozhenkov et al., *The Thomson scattering diagnostic at Wendelstein 7-X and its performance in the first operation phase*, 2017 *JINST* **12** P10004.

[9] J. Howard, B.W. James and W.I.B. Smith, *Rotational Raman calibration of Thomson scattering*, *J. Phys. D* **12** (1979) 1435.

2026 JINST 21 C02009

[10] E.T. Gerry and D.J. Rose, *Plasma Diagnostics by Thomson Scattering of a Laser Beam*, *J. Appl. Phys.* **37** (1966) 2715.

[11] B.P. LeBlanc, *Thomson scattering density calibration by Rayleigh and rotational Raman scattering on NSTX*, *Rev. Sci. Instrum.* **79** (2008) 10E737.

[12] I. Yamada et al., *Raman and Rayleigh Calibrations of the LHD YAG Thomson Scattering*, *Plasma and Fusion Research* **2** (2007) S1106.

[13] S.A. Bozhenkov et al., *On using Rayleigh scattering for in situ spectral calibration of Thomson scattering diagnostics*, *Rev. Sci. Instrum.* **90** (2019) 033505.

[14] E.R. Scott et al., *Demonstration of an absolute Rayleigh scattering spectral calibration on the W7-X Thomson scattering system*, 2019 *JINST* **14** C10033.

[15] R.B. Miles, W.R. Lempert and J.N. Forkey, *Laser Rayleigh scattering*, *Meas. Sci. Technol.* **12** (2001) R33.

[16] A. Börzsönyi et al., *Dispersion measurement of inert gases and gas mixtures at 800 nm*, *Appl. Opt.* **47** (2008) 4856.

[17] C.-A. Bunge, R. Kruglov and H. Poisel, *Rayleigh and Mie scattering in polymer optical fibers*, *J. Lightw. Technol.* **24** (2006) 3137.

[18] M. Lesiuk and B. Jeziorski, *First-principles calculation of the frequency-dependent dipole polarizability of argon*, *Phys. Rev. A* **107** (2023) 042805 [arXiv:2301.12502].

[19] M. Sneep and W. Ubachs, *Direct measurement of the Rayleigh scattering cross section in various gases*, *J. Quant. Spectrosc. Radiat. Trans.* **92** (2005) 293.

[20] R.R. Rudder and D.R. Bach, *Rayleigh Scattering of Ruby-Laser Light by Neutral Gases*, *J. Opt. Soc. Am.* **58** (1968) 1260.

[21] N.M. Kroll, *Parametric Amplification in Spatially Extended Media and Application to the Design of Tuneable Oscillators at Optical Frequencies*, *Phys. Rev.* **127** (1962) 1207.

[22] J.A. Giordmaine and R.C. Miller, *Tunable Coherent Parametric Oscillation in $LiNbO_3$ at Optical Frequencies*, *Phys. Rev. Lett.* **14** (1965) 973.

[23] S.A. Akhmanov and R.V. Khokhlov, *Parametric amplifiers and generators of light*, *Sov. Phys. Usp.* **9** (1966) 210.

[24] G. Fuchert et al., *Calibration techniques for Thomson scattering diagnostics on large fusion experiments*, *Rev. Sci. Instrum.* **95** (2024) 083533.

2026 JINST 21 C02009